MARMARA UNIVERSITY
INSTITUTE FOR GRADUATE STUDIES IN PURE AND APPLIED SCIENCES

CALCULATIONS OF HYPERPOLARIZABILITY AND TWO-PHOTON ABSORPTION CROSS SECTIONS OF ORGANIC CHARGE-TRANSFER COMPOUNDS

SHIVA MAHMOUDI

MASTER THESIS
Department of Physics

Thesis Supervisor
Prof. Dr. Erdi Ata BLEDA

Thesis Co- Supervisor
Prof. Dr. Zikri ALTUN

ISTANBUL, 2023

MARMARA UNIVERSITY
INSTITUTE FOR GRADUATE STUDIES IN PURE AND APPLIED SCIENCES

CALCULATIONS OF HYPERPOLARIZABILITY AND TWO-PHOTON ABSORPTION CROSS SECTIONS OF ORGANIC CHARGE-TRANSFER COMPOUNDS

SHIVA MAHMOUDI

(521220991)

MASTER THESIS
Department of Physics

Thesis Supervisor
Prof. Dr. Erdi Ata BLEDA

Thesis Co- Supervisor
Prof. Dr. Zikri ALTUN

ISTANBUL, 2023

MARMARA UNIVERSITY
INSTITUTE FOR GRADUATE STUDIES IN PURE AND APPLIED SCIENCES

Shiva MAHMOUDI, a Master of Science student of Marmara University Institute for Graduate Studies in Pure and Applied Sciences, defended her thesis entitled "**Calculations of Hyperpolarizability and Two-photon Absorption Cross Sections of Organic Charge-transfer Compounds** ", on and has been found to be satisfactory by the jury members.

Jury Members

Prof. Dr. Erdi Ata Bleda (Advisor)

Marmara University .....(SIGN) .....

Assist. Prof. Gülşen GÖRK (Jury Member)

Marmara University .....(SIGN) .....

Assist. Prof. Emrah KOÇ (Jury Member)

Istanbul Arel University .....(SIGN) .....

APPROVAL

Marmara University Institute for Graduate Studies in Pure and Applied Sciences Executive Committee approves that Shiva MAHMOUDI be granted the degree of Master of Science of Philosophy in Department of Physics, Physics Program on .
(Resolution no:).

Director of the Institute

ACKNOWLEGMENTS

First and foremost, I would like to thank my thesis advisor, Prof. Dr. Erdi A. Bleda for his guidance, insights, and encouragement throughout my studies and research. I am really grateful for his commitment and mentorship in shaping this thesis. May the Force be with him!

I would like to thank Prof. Dr. Zikri Altun for sharing his vast knowledge and experience with me and providing all the necessary tools and equipment to conduct this thesis.

Moreover, I express my gratitude to Prof. Dr. Carl Trindle for his invaluable contribution to this thesis. The development of this research would not have been possible without his expertise.

I would also like to mention that the numerical calculations reported in this thesis were partially performed at TUBITAK ULAKBIM, High Performance and Grid Computing Center (TRUBA resources).

Also, many thanks to my partner in crime for his understanding and support, and special thanks to V. Pakray for her omnipresent love, which was, is, and will be my driving force to succeed.

Finally, I am thankful to the physics faculty members of Marmara University.

May 2023 **Shiva MAHMOUDI**

TABLE OF CONTENTS

ÖZET

YÜK-TRANSFER ORGANİK BİLEŞİKLERDE HİPERPOLARİZASYON VE İKİ-FOTON SOĞURMA TESİR KESİT HESAPLAMALARI

Fizikteki en önemli konulardan biri, maddenin ışıkla etkileşimi ve bu etkileşimden kaynaklanan geçişlerdir. Kuantum mekaniği açısından, bu etkileşim, genellikle soğurulma gibi farklı süreçlere yol açabilecek bir geçişi tetikler. Bu soğurulma süreci genellikle taban halinden daha yüksek bir elektronik hale doğru gerçekleşir.

Işık yoğunluğu ve malzeme özellikleri ile ilgili olarak, doğrusal ve doğrusal olmayan soğurulma süreçleri vardır. Çoğu malzemelerde doğrusal soğurma süreci gerçekleşir. Ancak, bazı malzemeler, gelen ışığa doğrusal olmayan bir yanıt gösterir.

İki foton soğurma (TPA) süreci, üçüncü mertebeden doğrusal olmayan bir süreçtir. Bu süreç, düşük enerjili görünür veya yakın kızılötesi ışıkla yüksek enerjili elektronik hallerin uyarılması ile gerçekleşir. İki fotonun "aynı anda" soğrulması sonucu TPA gerçekleşir ve bu, iki fotonun ardışık soğurulmasından farklıdır.

TPA, tek foton spektroskopisini tamamlayıcı bir teknik olarak, moleküler elektronik yapı hakkında bilgi edinmek için kullanılabilir. Uygulamalı alanda, iki foton litografi, veri depolama, hücre görüntüleme ve tıbbi konularda, biyolojik dokulara daha iyi nüfuz etme özelliği sayesinde, kullanılabilir. Vücut dokusu düşük enerjili ışığa yarı saydam olduğundan, büyük TPA kesiti olan moleküllerle işaretlenmiş tümörlere enerji taşınması mümkündür.

Büyük TPA kesitine sahip organik sistemler genellikle X-B-Y yapısına sahiptir, B, X ve Y fragmentlerini bağlayan, elektron akseptör (A) veya elektron donörleri (D) köprüsüdür. Bu tezde, sülfür atomunu bir köprü olarak kullanıp donör ve akseptör parçalarını bağladığımız dört farklı küçük molekül için TPA kesitlerini hesapladık.

ABSTRACT

CALCULATIONS OF HYPERPOLARIZABILITY AND TWO-PHOTON ABSORPTION CROSS SECTIONS OF ORGANIC CHARGE-TRANSFER COMPOUNDS

One of the most important topics in physics is the study of matter and its interaction with light. Quantum mechanically speaking, due to this interaction, a transition happens which may lead to different phenomena such as absorption. This absorption process usually occurs from the ground state to a higher electronic state.

Regarding the intensity of the light and properties of the materials, there are linear and nonlinear absorption processes. Linear absorption occurs in most materials. However, certain materials show a nonlinear response to the incident light.

The two-photon absorption is a third order nonlinear process. This process can populate highly energetic electronic states by irradiating them with low-energy visible or near-infrared light. TPA happens when two photons are absorbed simultaneously, which makes it different from the sequential absorption of two photons.

TPA can be used to gain information on molecular electronic structure as a complementary technique to one-photon spectroscopy. Practical applications have already been established in two-photon lithography, data storage, cell imaging, and medicine because of its enhanced ability to penetrate biological tissue. Since body tissue is semi-transparent to low-energy light, the delivery of energy through the body to targets such as tumors labeled by molecules with a large two-photon absorption (TPA) cross section would be possible.

Organic systems with large TPA cross-sections often have the structure X-B-Y, with B being a bridge connecting fragments X and Y, electron acceptors (A) or electron donors (D). In this thesis, we report our calculated TPA cross sections for four small molecules with the sulfur atom as a bridge to link donor and acceptor moieties.

SYMBOLS

$\hat{H}$	:Hamiltonian operator
E_{tot}	:Total energy of the system
Ψ	:Wave function
$\vec{x} = \{\vec{r}, \omega\}$	:Coordinate of an electron with its spin
$\alpha(\omega)$	:Spin up
$\beta(\omega)$	:Spin down
$\hat{h}(i)$	:One electron Hamiltonian
χ_j	:Eigen functions
E_0	:Lowest energy of the system
δE	:Linear variation
$\hat{J}$	:Coulomb operator
$\hat{K}$	:Exchange operator
$\hat{f}$	:Fock operator
$\tilde{\epsilon}_a$	:Orbital energy
$\tilde{\chi}_\mu$	:Basis functions
$C_{\mu i}$	:Expansion coefficients
S	:Overlap matrix
F	:Fock matrix
$\rho(\vec{r})$	:Total electron density at point ($\vec{r}$)
T	:Kinetic energy
$\phi_i(\vec{r})$	:Kohn-Sham orbitals
E_{XC}	:Exchange-correlation energy
V_{XC}	:Exchange-correlation potential
P_i	:Polarization
$\chi_{ij}^{(1)}$	:Linear susceptibility
$\chi_{ijk}^{(2)}$	:Second-order nonlinear susceptibility
$\chi_{ijkl}^{(3)}$	:Third-order nonlinear susceptibility
μ_i^{ind}	:Induced dipole moment
α_{ij}	:Linear polarizability
β_{ijk}	:First hyperpolarizability

$\boldsymbol{\gamma_{ijkl}}$:Second hyperpolarizability

$\hbar$:Reduced Planck constant

$\boldsymbol{\alpha_f}$:Fine structure constant

$\boldsymbol{\sigma_{TPA}}$:Two-photon absorption cross section

$\boldsymbol{f}$:Oscillator strength

ABBREVIATIONS

TPA : Two-Photon Absorption
OPA : One-Photon Absorption
HOMO : Highest Occupied Molecular Orbital
LUMO : Lowest Unoccupied Molecular Orbital
GM : Goeppert-Mayer
BO : Born-Oppenheimer
HF : Hartree-Fock
LCAO : Linear Combination of Atomic Orbital
SCF : Self-Consistent Field
STO : Slater-Type Orbital
GTO : Gaussian-Type Orbital
DZ : Double-Zeta
TZ : Triple-Zeta
DFT : Density Functional Theory
TDDFT : Time-Dependent Density Functional Theory
KS : Kohn-Sham
MP2 : Møller–Plesset Perturbation Theory of Second Order
NTO : Natural Transition Orbital

LIST OF FIGURES

LIST OF TABLES

1. INTRODUCTION

When light interacts with matter (atom, molecule, etc.), it gives rise to a range of phenomena such as absorption, reflection, scattering, or emission of light. The study of the interaction of light with matter is one of the most studied aspects of physics and has broad applications in many other scientific and engineering fields.

The interaction of light with matter is a complex phenomenon and is governed by the principles of quantum mechanics. When a photon of light interacts with an atom, it can be absorbed provided that the energy of the photon matches the difference between any of the two energy levels of the atom. If this occurs, the atom can be excited to a higher energy level with a high probability.

In this thesis, we study an optical phenomenon known as Two-Photon Absorption (TPA). TPA is a nonlinear process that was first proposed by Maria Goeppert-Mayer in 1931 [1] . She suggested that two photons could be "simultaneously" absorbed by an atom (or molecule), with the energy of each photon being half of the total energy required for an electronic transition between energy states in the atom (or molecule) as seen in Figure 1.

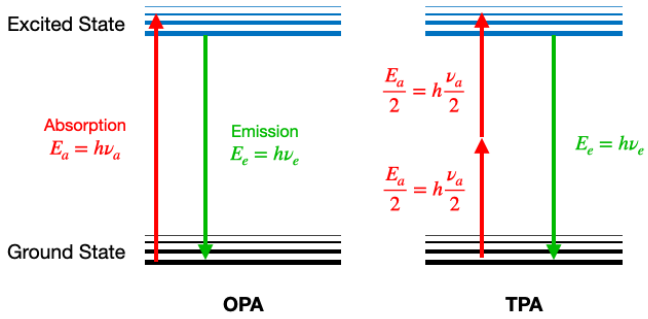

Figure 1. *Representations of One-Photon and Two-Photon Absorption Processes*

This is different from One-Photon Absorption (OPA) where an atom (or molecule) absorbs only one photon of light to make a transition. The probability of TPA occurring compared to OPA is quite small, which means that the intensity of the applied optical fields has to be very high in order to observe TPA. However, experimental confirmation of TPA awaited for almost thirty years until the advent of lasers which provided a way to generate the required high intensity optical fields. In 1961, W. Kaiser and C.G.B. Garret were able to perform the first observation of TPA using lasers [2].

The continuous advancements in laser technology have opened up new possibilities for exploring the potential applications of TPA. Some of the notable developments in this area include the use of TPA for microfabrication [3,4] , three-dimensional data storage [5], microscopy [6,7], and particularly, its promising results in the treatment of various diseases through photodynamic therapy [8,9,10]. As researchers continue to delve deeper into the properties of TPA, new and exciting applications are expected to emerge in the future.

The TPA cross sections are related to the imaginary part of the third-order susceptibility tensor which is a macroscopic quantity. However, when dealing with molecules, the second hyperpolarizability tensor γ, which is a microscopic quantity, is more useful in relation to TPA cross section calculations [11].

Given the considerable demand for efficient TPA processes spanning a wide range of applications, the identification and design of suitable chromophores play a pivotal role. Several key requirements must be met to maximize the two-photon absorption cross section, as outlined in [11,12,13]:

- Long, π conjugated molecular structure to extend the charge separation.
- An enforced coplanarity to enhance the intramolecular charge transfer.
- A small HOMO-LUMO gap to enhance the hyperpolarizability.
- Presence of donor (D) and acceptor (A) at the center and ends of the molecule to increase the intramolecular charge transfer.

In this thesis, we calculated TPA cross sections for four molecules (ASA, DSD, DSA, and $DSAPh^{+}$) whose molecular structures and their coordinates of the optimized geometries are given in Section 3: *Materials and Method*. In these structures, a sulfur atom, which can act as an acceptor (A) or as a donor (D), is used to link donor and acceptor fragments. In order to calculate the cross sections, computational quantum chemistry programs capable of calculating the second hyperpolarizability tensor are necessary. We used DFT method for calculating the molecular properties.

In Section 2: *Theory*, we introduce some of the techniques and approximations used to solve a many-body Hamiltonian and how they help us to gain insight into the behavior of atoms and molecules. In Section 4: *Results and Discussion*, we explain the computational results based on our chosen exchange-correlation functional and basis set.

2. THEORY

2.1 The Born-Oppenheimer Approximation

In quantum mechanics of many-body systems, we usually encounter Schrödinger's equation, which cannot be solved exactly. Therefore, it is essential to develop approximate solutions to this equation. The non-relativistic, time-independent Schrödinger equation can be expressed as follows:

$$\hat{H} = -\sum_{i=1}^{N}\frac{1}{2}\nabla_i^2 - \sum_{A=1}^{M}\frac{1}{2M_A}\nabla_A^2 - \sum_{i=1}^{N}\sum_{A=1}^{M}\frac{Z_A}{r_{iA}} + \sum_{i=1}^{N}\sum_{j>i}^{N}\frac{1}{r_{ij}} + \sum_{A=1}^{M}\sum_{B>A}^{M}\frac{Z_A Z_B}{R_{AB}}. \quad (1)$$

Here, Z_A is the atomic number and M_A is the mass of the nucleus A in atomic units. The coordinate representation of a many-body system (say a molecule) is given in Figure 2. The first term in Eq.1 represents the total kinetic energy of the electron whereas the second term represents total kinetic energy of the nuclei. The remaining terms represent the potential energies of electron-nucleus, electron-electron, and nucleus-nucleus interactions, respectively.

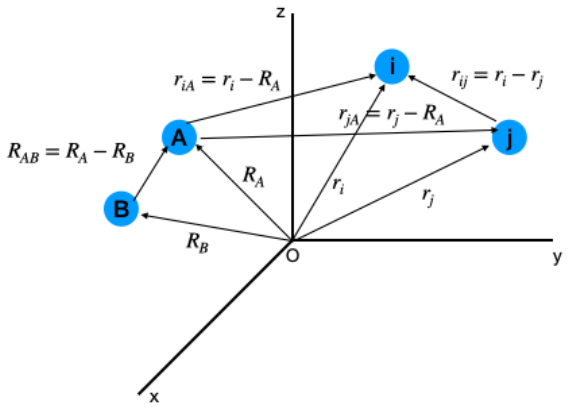

Figure 2. *A molecular coordinate representation where i and j are electrons and A and B are nuclei*

Even for the simplest molecular system such as H_2^+, Eq.1 cannot be solved analytically. The coupling of electronic motion to nuclear motion can even make the problem more complicated. One of the simplifications commonly employed here is known as Born-Oppenheimer (BO) approximation. In this approximation, the electronic motions and the nuclear motions are decoupled by the assumption that nuclei respond much slower to the electronic motion due to their mass to electron mass ratio. This assumption has established great acceptance in computational many-body physics and chemistry [14,15].

Under BO approximation, the Hamiltonian representing the electronic motion can be written as

$$\widehat{H}_{el} = -\sum_{i}^{N}\frac{1}{2}\nabla_i^2 - \sum_{i=1}^{N}\sum_{A=1}^{M}\frac{Z_A}{r_{iA}} - \sum_{i=1}^{N}\sum_{j>i}^{N}\frac{1}{r_{ij}}. \tag{2}$$

Hence the corresponding Schrodinger's equation is

$$\left[-\sum_{i}^{N}\frac{1}{2}\nabla_i^2 - \sum_{i=1}^{N}\sum_{A=1}^{M}\frac{Z_A}{r_{iA}} - \sum_{i=1}^{N}\sum_{j>i}^{N}\frac{1}{r_{ij}}\right]\Psi_{el}\left(\{\vec{r}_i\};\{\vec{R}_A\}\right) = E_{el}\left(\{\vec{R}_A\}\right)\Psi_{el}\left(\{\vec{r}_i\};\{\vec{R}_A\}\right). \tag{3}$$

We should mention that in Eq.3, the set of coordinates $\{\vec{r}_i\}$ and $\{\vec{R}_A\}$ represent the positions of electrons and the positions of the nuclei, respectively. Here, the nuclei positions $\{\vec{R}_A\}$ are fixed, thus they just serve as a set of parameters for the solution of the electronic motion. The remaining term in the Hamiltonian is the nuclei-nuclei interaction term, which is simply a constant under BO approximation for the electronic solution. This would only shift the electronic energy, allowing us to write the total energy for a fixed set of nuclei positions, as

$$E_{tot}\left(\{\vec{R}_A\}\right) = E_{el}\left(\{\vec{R}_A\}\right) + \sum_{A=1}^{M}\sum_{B>A}^{M}\frac{Z_A Z_B}{R_{AB}}. \tag{4}$$

In the above statement, we should clarify that under BO approximation, the kinetic energy of the nuclei is negligible compared to that of the electrons.

If we look at the Hamiltonian for the nuclear motion, due to the reason that the electrons move much faster than the nuclei, it is only reasonable to use the average value of the electronic Hamiltonian. As a result of this, the Hamiltonian for the nuclear motion becomes

$$\widehat{H}_{nuc} = -\sum_{A=1}^{M}\frac{1}{2M_A}\nabla_A^2 + \left\langle -\sum_{i=1}^{N}\frac{1}{2}\nabla_i^2 - \sum_{i=1}^{N}\sum_{A=1}^{M}\frac{Z_A}{r_{iA}} + \sum_{i=1}^{N}\sum_{j>i}^{N}\frac{1}{r_{ij}}\right\rangle + \sum_{A=1}^{M}\sum_{B>A}^{M}\frac{Z_A Z_B}{R_{AB}} \tag{5}$$

$$= -\sum_{A=1}^{M} \frac{1}{2M_A} \nabla_A^2 + E_{el}\left(\{\vec{R}_A\}\right) + \sum_{A=1}^{M} \sum_{B>A}^{M} \frac{Z_A Z_B}{R_{AB}}$$

$$= -\sum_{A=1}^{M} \frac{1}{2M_A} \nabla_A^2 + E_{tot}\left(\{\vec{R}_A\}\right).$$

Here, we should immediately see that the total energy $E_{tot}\left(\{\vec{R}_A\}\right)$ in Eq.5 behaves as a potential that governs the nuclear motion. Figure 3 shows how $E_{tot}\left(\{\vec{R}_A\}\right)$ varies with respect to $\{\vec{R}_A\}$.

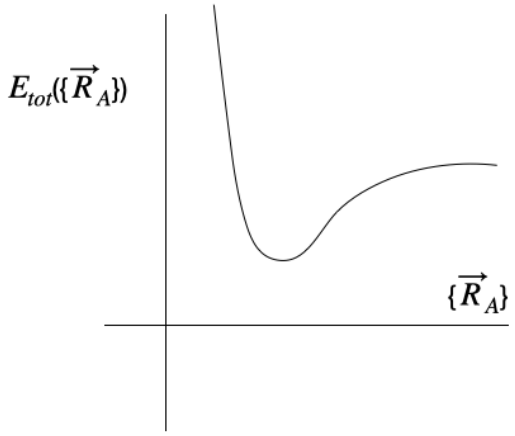

Figure 3. *Symbolic representation of a potential energy surface*

The Schrodinger's equation for the nuclear motion,

$$\hat{H}_{nuc} \Psi_{nuc}\left(\{\vec{R}_A\}\right) = E \Psi_{nuc}\left(\{\vec{R}_A\}\right), \tag{6}$$

describes the translational, rotational and vibrational motion of the many-body system. Finally, the wave function describing this many-body system under BO approximation can be written as

$$\Psi\left(\{\vec{r}_i\}; \{\vec{R}_A\}\right) = \Psi_{nuc}\left(\{\vec{R}_A\}\right) \Psi_{el}\left(\{\vec{r}_i\}; \{\vec{R}_A\}\right). \tag{7}$$

2.2 The Hartree-Fock Method

The Hamiltonian given in Eq.2 only depends on the spatial coordinates and makes no reference to electron spins. However, any wave function representing a real multi-electron system must also include

spins. To introduce spin to the wave function, we introduce spin functions $\alpha(\omega)$ and $\beta(\omega)$, where ω is a unspecified spin variable, corresponding to "up" and "down" spins. We also require these functions satisfy the completeness and orthonormality conditions. We can now couple the coordinate of an electron with its spin function as

$$\vec{x} = \{\vec{r}, \omega\} \tag{8}$$

However, this still doesn't solve the antisymmetry problem of the wave function, that is– any multi-electron wave function must change sign upon interchange of any pair of its coordinates. This is known as the *antisymmetry principle* and written as

$$\Psi(\vec{x}_1, \vec{x}_2, \dots, \vec{x}_i, \dots, \vec{x}_j, \dots x_{N-1}, \vec{x}_N) = -\Psi(\vec{x}_1, \vec{x}_2, \dots, \vec{x}_j, \dots, \vec{x}_i, \dots, \vec{x}_{N-1}, \vec{x}_N). \tag{9}$$

We define *orbital* as the wave function that describes a single electron. This wave function is denoted as a pure spatial function, represented by $\psi(\vec{r})$. However, in order to represent an electron accurately, we must also include its spin in the wave function. With the introduction of the complete spin set $\alpha(\omega)$ and $\beta(\omega)$, we can now define *spin-orbital as*

$$\chi(\vec{x}) = \begin{cases} \psi(\vec{r})\alpha(\omega) \\ \text{or} \\ \psi(\vec{r})\beta(\omega) \end{cases}, \tag{10}$$

which fully describes both the spatial and spin properties of an electron.

For a moment, let's consider a system containing N non-interacting electrons. The Hamiltonian for such a system can be written as

$$\hat{H} = \sum_{i=1}^{N} \hat{h}(i), \tag{11}$$

where $\hat{h}(i)$ is called one-electron Hamiltonian which is consist of the kinetic and the potential energy of a single electron. This Hamiltonian is exact for non-interacting electrons. For the case of interacting electrons, this Hamiltonian cannot represent the system accurately, however, it can still serve as an "effective" Hamiltonian. The electron-electron repulsion can be included as the average field on the i^{th} electron due to all other electrons.

Now, let's look at the eigenfunctions $\{\chi_j\}$ of the one-electron Hamiltonian given in Eq.11,

$$\hat{h}(i)\chi_j(\vec{x}_i) = \epsilon_j\chi_j(\vec{x}_i) \tag{12}$$

Since the total Hamiltonian is the sum of all these one-electron Hamiltonians, the eigenfunctions of the total Hamiltonian is simply the product of all the eigenfunctions of the one-electron Hamiltonian. Hence, the wave function is

$$\Psi_{\mathrm{HP}}(\vec{x}_1, \vec{x}_2, \dots, \vec{x}_N) = \chi_i(\vec{x}_1)\chi_j(\vec{x}_2)\dots\chi_k(\vec{x}_N). \tag{13}$$

"HP" in Eq.13 stands for "Hartree Product".

The Hartree Product wave function given in Eq.13 still suffers from the antisymmetry principle. We already know that any linear combination of the solutions of a linear differential equation is also a solution of the differential equation. Hence, we can look for a very special linear combination that satisfies the antisymmetry principle. This linear combination is known as *Slater Determinant* and given as

$$\Psi(\vec{x}_1, \vec{x}_2, \dots, \vec{x}_N) = \frac{1}{\sqrt{N!}}\begin{vmatrix} \chi_i(\vec{x}_1) & \chi_j(\vec{x}_1) & \cdots & \chi_k(\vec{x}_N) \\ \chi_i(\vec{x}_2) & \chi_j(\vec{x}_2) & \cdots & \chi_k(\vec{x}_N) \\ \vdots & \vdots & & \vdots \\ \chi_i(\vec{x}_N) & \chi_j(\vec{x}_N) & \cdots & \chi_k(\vec{x}_N) \end{vmatrix} \tag{14}$$

Here, the $1/\sqrt{N!}$ factor is the normalization necessary for the normalization of the wave function Ψ. It is clearly seen that this linear combination satisfies the antisymmetry principle.

Now, let's look at an N interacting electron system. The Hamiltonian for the system can be written as

$$\begin{aligned} \hat{H} &= \sum_{i=1}^{N} \hat{h}\,(i) \\ &= \sum_{i=1}^{N}\left[\underbrace{-\frac{1}{2}\nabla_i^2 + \sum_{A=1}^{N}\frac{Z_A}{|\vec{r}_{iA}|}}_{\hat{h}_1(i)} + \frac{1}{2}\sum_{\substack{j=1 \\ j\neq i}}^{N}\underbrace{\frac{1}{|\vec{r}_i - \vec{r}_j|}}_{\hat{h}_2(i,j)}\right] \end{aligned} \tag{15}$$

Here, $\hat{h}_1$ is the one-electron operator and $\hat{h}_2$ is the two-electron operator. We can calculate the energy of this system using a wavefunction expressed as a single Slater determinant as

$$E = \langle \Psi | \hat{H} | \Psi \rangle. \tag{16}$$

We can rewrite Eq.16 as

$$E = \sum_{a=1}^{occ} \langle a | \hat{h}_1 | a \rangle + \frac{1}{2} \sum_{a=1}^{occ} \sum_{b=1}^{occ} [\langle ab|ab\rangle - \langle ab|ba\rangle] \tag{17}$$

where $|a\rangle = \chi_a$. The $\langle ab|ab\rangle$ seen in the double summation is called the *Coulomb integral* and it is given as

$$\langle ab|ab\rangle = \iint d\vec{x}_1 d\vec{x}_2 \chi_a^*(\vec{x}_1)\chi_b^*(\vec{x}_2)\hat{h}_2(1,2)\chi_a(\vec{x}_1)\chi_b(\vec{x}_2), \tag{18}$$

and $\langle ab|ba\rangle$ is called the *exchange integral* and it is given as

$$\langle ab|ba\rangle = \iint d\vec{x}_1 d\vec{x}_2 \chi_a^*(\vec{x}_1)\chi_b^*(\vec{x}_2)\hat{h}_2(1,2)\chi_b(\vec{x}_1)\chi_a(\vec{x}_2). \tag{19}$$

We should mention that since electrons are indistinguishable, $\vec{x}_1$ and $\vec{x}_2$ are chosen just for convenience.

We now have the expression for the energy, let's calculate the ground state energy of an N interacting electron system. In Hartree-Fock theory, the wave function of the system is expressed as a Slater determinant which consists of mutually orthonormal one electron spin orbitals. However, these orbitals are yet to be identified. One can immediately realize that energy $E[\Psi]$ is indeed a functional of the wave function Ψ. We know that

$$\langle \Psi | \hat{H} | \Psi \rangle \geq E_0, \tag{20}$$

where E_0 is the lowest energy, the system is allowed to have. Hence one can find a set of equations, which gives a set of spin orbitals that correctly identities the system, by minimizing the energy functional $E[\Psi]$ on varying the wave function $\Psi \to \Psi + \delta\Psi$.

$$\begin{aligned} E[\Psi + \delta\Psi] &= \langle \Psi + \delta\Psi | \hat{H} | \Psi + \delta\Psi \rangle \\ &= E[\Psi] + \underbrace{\{\langle \delta\Psi | \hat{H} | \Psi \rangle + \langle \Psi | \hat{H} | \delta\Psi \rangle\}}_{\delta E} + \cdots. \end{aligned} \tag{21}$$

Here, the term δE is the linear variation, and for a minimum, this needs to be zero. After lengthy calculations, we end up with the following equation:

$$\left[\underbrace{\hat{h}_1(1) + \sum_{b=1}^{occ}\left(\hat{J}_b(\vec{x}_1) - \hat{K}_b(\vec{x}_1)\right)}_{\hat{f}}\right]\chi_a(\vec{x}_1) = \sum_{b=1}^{occ}\epsilon_{ab}\chi_b(\vec{x}_1), \tag{22}$$

where $\hat{J}$ and $\hat{K}$ are given as

$$\hat{J}_b(\vec{x}_1)\chi_a(\vec{x}_1) \equiv \left\{\int d\vec{x}_2\chi_b^*(\vec{x}_2)\hat{h}_2(1,2)\chi_b(\vec{x}_2)\right\}\chi_a(\vec{x}_1) \tag{23}$$

$$\hat{K}_b(\vec{x}_1)\chi_a(\vec{x}_1) \equiv \left\{\int d\vec{x}_2\chi_b^*(\vec{x}_2)\hat{h}_2(1,2)\chi_a(\vec{x}_2)\right\}\chi_b(\vec{x}_1).$$

The $\hat{J}$ operator is called the *Coulomb operator* and the $\hat{K}$ operator is called the *exchange operator*. The one-electron operator inside the square bracket in Eq.22 is called the Fock operator $\hat{f}$, which leads to the Hartree-Fock equations in the non-canonical form and are written as

$$\hat{f}|\chi_a\rangle = \sum_{b=1}^{N}\epsilon_{ab}|\chi_b\rangle. \tag{24}$$

This is not yet an eigenvalue-eigenvector problem since $\boldsymbol{\epsilon}$ is not diagonal. However, $\boldsymbol{\epsilon}$ is hermitian, which means that with a proper unitary transformation $\widehat{\boldsymbol{U}}$, $\boldsymbol{\epsilon}$ can be diagonalized. Applying the unitary transformation that diagonalizes $\boldsymbol{\epsilon}$ to the spin orbitals would make a new set of spin orbitals, which are nothing but a linear combination of the original set. Spin orbitals obtained in this fashion clearly would not alter the Slater determinant. If we define the new of spin orbitals as

$$|\chi_a'\rangle = \sum_{k=1}^{N}|\chi_k\rangle U_{kl}, \tag{25}$$

then we can define a row vector of new spin orbitals as

$$\boldsymbol{\chi}' = (|\chi_1'\rangle\ |\chi_2'\rangle \dots |\chi_a'\rangle \dots |\chi_N'\rangle) \tag{26}$$

Hence, Eq.24 can be written as

$$\hat{f}\boldsymbol{\chi}' = \boldsymbol{\chi}'\boldsymbol{\epsilon} \tag{27}$$

$$\hat{f}\underbrace{\boldsymbol{\chi}'\boldsymbol{U}}_{\tilde{\boldsymbol{\chi}}} = \underbrace{\boldsymbol{\chi}'\boldsymbol{U}}_{\tilde{\boldsymbol{\chi}}}\underbrace{\boldsymbol{U}^{\dagger}\boldsymbol{\epsilon}\boldsymbol{U}}_{\tilde{\boldsymbol{\epsilon}}}.$$

In the above equation, $\tilde{\boldsymbol{\epsilon}}$ is diagonal. This enables us to write Eq.24 as

$$\hat{f}|\tilde{\chi}_a\rangle = \tilde{\epsilon}_a|\tilde{\chi}_a\rangle. \tag{28}$$

Eq.28 is the canonical form of the Hartree-Fock equations. $\tilde{\epsilon}_a$ is called orbital energy.

2.2.1 The Basis Set Approximation

Each spatial molecular orbital can be expanded from a linear combination of atomic orbital (LCAO) basis functions $|\tilde{\chi}_\mu\rangle$ as

$$|\chi_i\rangle = \sum_{\mu=1}^{N_{bas}} |\tilde{\chi}_\mu\rangle C_{\mu i}, \tag{29}$$

which transforms the Hartree-Fock equations into the Roothaan-Hall equations. Here, the N_{bas} is the number of basis functions and $C_{\mu i}$ are the expansion coefficients. Therefore, Eq. 28 may be written as

$$\hat{f}\sum_{\mu=1}^{N_{bas}} |\tilde{\chi}_\mu\rangle C_{\mu i} = \epsilon_i \sum_{\mu=1}^{N_{bas}} |\tilde{\chi}_\mu\rangle C_{\mu i} \tag{30}$$

We can obtain a matrix equation by multiplying both sides by $\langle\tilde{\chi}_\nu|$ and integrating,

$$\sum_{\mu=1}^{N_{bas}} C_{\mu i}\langle\tilde{\chi}_\nu|\hat{f}|\tilde{\chi}_\mu\rangle = \epsilon_i \sum_{\mu=1}^{N_{bas}} C_{\mu i}\langle\tilde{\chi}_\nu|\tilde{\chi}_\mu\rangle \tag{31}$$

In order to simplify Eq.31, we can define the elements of *overlap matrix* $\boldsymbol{S}$ as

$$S_{\nu\mu} = \langle\tilde{\chi}_\nu|\tilde{\chi}_\mu\rangle, \tag{32}$$

and the elements of the *Fock matrix* $\boldsymbol{F}$ as

$$F_{\nu\mu} = \langle\tilde{\chi}_\nu|\hat{f}|\tilde{\chi}_\mu\rangle. \tag{33}$$

Eq.31 can be expressed even in a more compressed way,

$$\sum_{\mu=1}^{N_{bas}} F_{\nu\mu} C_{\mu i} = \epsilon_i \sum_{\mu=1}^{N_{bas}} S_{\nu\mu} C_{\mu i}, \tag{34}$$

which leads to the form

$$\boldsymbol{FC} = \boldsymbol{SC\epsilon} \tag{35}$$

where $\boldsymbol{\epsilon}$ is a diagonal matrix of the orbital energies ϵ_i, $\boldsymbol{S}$ is the overlap matrix containing overlap elements between basis functions, and $\boldsymbol{F}$ is the Fock matrix. Each element of the Fock matrix contains two parts from the Fock operator, one-electron integrals, and a sum over occupied MOs of coefficients multiplied by two-electron integrals involving the electron–electron repulsion. The latter is often written as a product of a *density* matrix and two-electron integrals [16].

In order to find out the coefficients $C_{\mu i}$, the diagonalization of the Fock matrix is necessary. The procedure is done iteratively by guessing the coefficients to form the Fock matrix and diagonalizing it. Then, in order to calculate the new Fock matrix, the new coefficients are used. This procedure continues to the point that the generating orbitals are self-consistent with the Fock matrix they generate. This is why the procedure, which is used to solve the Hartree-Fock-Roothaan equations, is called the self-consistent field (SCF) method and is illustrated in Figure 4.

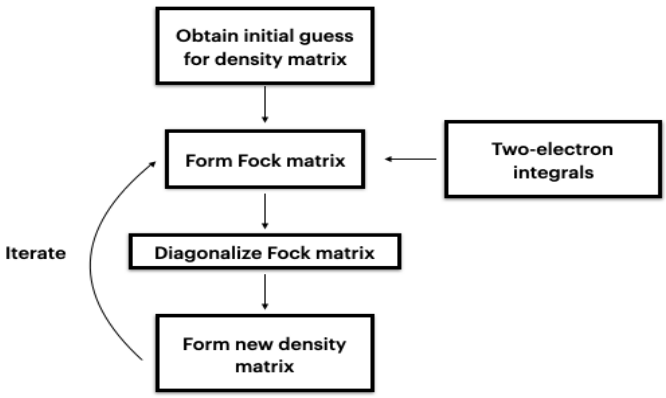

Figure 4. *Illustration of the SCF procedure*

There are two other crucial factors which need to be considered in these calculations: the introduction of a basis set, and the type of basis functions that will affect the accuracy of the calculations. In electronic structure calculations, *Slater Type Orbitals (STO)* and *Gaussian Type Orbitals (GTO)* are the common basis functions which are used. Then, the type of basis set needs to be chosen. There are

different types of basis sets such as the minimal basis set which has one basis function for each atomic orbital in the atom, the double-zeta (DZ), the triple-zeta (TZ), and so on.

2.3 Density Functional Theory

An alternative to the HF method is the Density Functional Theory (DFT), in which correlations between electrons are considered.

The basic idea of DFT is to express the electronic system in terms of the electron density. For a system of N electrons, $\rho(\vec{r})d^3\vec{r}$ is the electron density in an infinitesimal volume element $d^3\vec{r}$ located at $\vec{r}$ in real space. So, the electronic energy E can be determined as a functional of this electron density $E[\rho]$. Consequently, we only need to know the electron density to determine the energy functional in order to obtain the ground-state energy of the system. The advantage of using the electron density is that even for many-body systems, it is a function of three-dimensional space. Moreover, the Schrödinger equation may be expressed by a system of independent electrons whose electron density is similar to that of a system with interacting electrons.

Two theorems by Hohenberg and Kohn for the nondegenerate ground electronic state can be considered as the foundation for density functional theory [17]. The first theorem states that the ground-state electron density uniquely determines the external potential of a system, which corresponds to the nuclear-electron interaction potential in the absence of an electromagnetic field, up to an additive constant. The second theorem proves the variational principle by expressing that the electron density of a system is the one which minimizes the total energy of the system. Unfortunately, the exact form of the functional is not known. As a result, it is obvious that we still need to make approximations.

To start off, the electronic energy of a molecule can be expressed as a functional of the electron density $\rho\ as$,

$$E[\rho] = T[\rho] + E_{ne}[\rho] + J[\rho] + E_{XC}[\rho], \tag{36}$$

where T is the kinetic energy of non-interacting electrons, E_{ne} is the nuclear-electron attraction, and J is the Coulomb part of the electron-electron repulsion energy. The exchange and the electron correlations are absorbed in the exchange-correlation functional E_{XC}.

E_{ne} and J in Eq.36 are already known in terms of the electron density. E_{ne} can be expressed as,

$$E_{ne} = -\sum_{A=1}^{M} \int \frac{\rho(\vec{r})}{r_A} d^3\vec{r} \tag{37}$$

Where r_A is the distance relative to the position of nucleus A, and M is the number of nuclei. We can rewrite the Coulomb term J in terms of electron density by recalling the HF energy expression,

$$J = \frac{1}{2}\iint \rho(\vec{r}_1)\frac{1}{r_{12}}\rho(\vec{r}_2)d^3\vec{r}_1 d^3\vec{r}_2 \tag{38}$$

where $\vec{r}_1$ and $\vec{r}_2$ are the positions of electrons 1 and 2 and r_{12} is the distance between these two electrons. For the electrons, a Coulomb potential can be defined as

$$V_C(\vec{r}_1) = \int \frac{\rho(\vec{r}_2)}{r_{12}} d^3\vec{r}_2 \tag{39}$$

So J is simplified as

$$J = \frac{1}{2}\int \rho(\vec{r})V_C(\vec{r})d^3\vec{r} \tag{40}$$

The exchange-correlation functional E_{XC}, is then defined relative to the Coulomb repulsion term J to obtain the exact electronic energy. We need to point out that since the kinetic energy term is for non-interacting electrons, the corrections due to many-body interaction of the electrons are also included in the exchange-correlation functional. In general, the approximations are used for $E_{XC}[\rho]$ functional.

Kohn and Sham proposed that the exact electron density may be defined as a set of spatial one-electron functions $\phi_i(\vec{r})$ which are called Kohn-Sham (KS) orbitals [18].

$$\rho(\vec{r}) = \sum_{i=1}^{N/2} n_i |\phi_i(\vec{r})|^2 \tag{41}$$

where n_i is the number of electrons occupying the i^{th} orbital. So, the KS energy functional is expressed as

$$E = \sum_{i=1}^{N/2} n_i \langle\phi_i| -\frac{1}{2}\nabla^2|\phi_i\rangle - \sum_{A=1}^{M} Z_A \int \frac{\rho(\vec{r})}{r_A} d^3\vec{r} + \frac{1}{2}\int \rho(\vec{r})V_C(\vec{r})d^3\vec{r} + E_{XC}[\rho]. \tag{42}$$

The KS equations can also be expressed as an eigenvalue equation,

$$\hat{f}\phi_i = \epsilon_i \phi_i \tag{43}$$

with $\hat{f}$ being the KS Fock operator,

$$\hat{f} = \hat{h} + V_C + V_{XC}[\rho] \tag{44}$$

$$\hat{f} = \hat{h} + 2\sum_{j=1}^{N} \hat{J}_j + V_{XC} \tag{45}$$

Therefore, in order to calculate the total electronic energy in the Kohn-Sham method, we use the exchange-correlation energy functional as

$$E = \sum_{i=1}^{N} \left(h_i + 2\sum_{j=1}^{N} J_{ij} \right) + E_{XC} \tag{46}$$

So, the exchange-correlation functional V_{XC} is

$$V_{XC} = \frac{\delta E_{XC}}{\delta \rho}. \tag{47}$$

2.3.1 Exchange-Correlation Functionals

The search for an accurate form for the functional to obtain the exchange-correlation energy is an area of research efforts. As it can be seen in Figure 5, there are different types of functionals. These functionals usually have two parts: the first part is an exchange functional which represents exchange energy, and the second part, which represents correlation energy, is known as a correlation functional. There are a variety of exchange-correlation functionals such as BLYP, PBE1PBE, PWPW91, B1B95, and PBE that have been developed to do DFT calculations [19]. Some of the functionals such as B3LYP use Hartree-Fock corrections with DFT correlation-exchange term and are called hybrid.

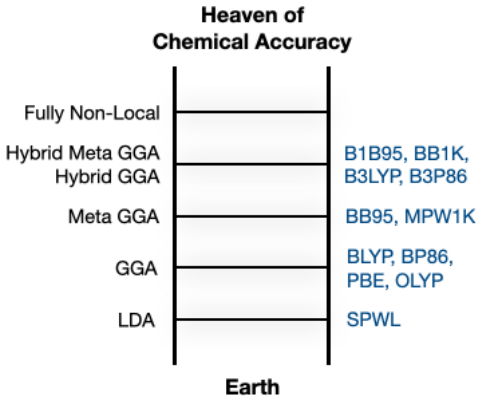

Figure 5. *Jacob's ladder for DFT functionals, with some of the most common DFT functionals in each rung*

2.4 TPA Cross Section

When we deal with light-matter interaction, we can expand induced polarization in terms of the applied electric field for a lot of practical nonlinear applications.

$$P_i = \chi_{ij}^{(1)} E_j + \chi_{ijk}^{(2)} E_j E_k + \chi_{ijkl}^{(3)} E_j E_k E_l + \cdots \tag{48}$$

Here $\chi_{ij}^{(1)}$ is the first-order (linear) susceptibility, which is a second-rank tensor, and its imaginary part is used to determine the one-photon absorption. The other terms $\chi_{ijk}^{(2)}$ and $\chi_{ijkl}^{(3)}$ describe nonlinear responses of the material. $\chi_{ijkl}^{(3)}$ is the third-order nonlinear susceptibility and a fourth-rank tensor. We use its imaginary part to describe the two-photon absorption phenomenon.

However, on the molecular scale, it is more convenient to replace susceptibilities, which are macroscopic coefficients, with the microscopic (hyper) polarizabilities. To clarify more, we know that the laser field is described as an oscillating electromagnetic field of photons and therefore, in its presence, the motion of all charged particles in a molecule is perturbed. The oscillating charges in the molecule cause an induced dipole moment. The expansion of the induced dipole is expressed as

$$\mu_i^{ind} = \alpha_{ij} E_j + \frac{1}{2}\beta_{ijk} E_j E_k + \frac{1}{6}\gamma_{ijkl} E_j E_k E_l \tag{49}$$

where α_{ij} is the polarizability of the molecule, β_{ijk} is the first molecular hyperpolarizability, and γ_{ijkl} is the second molecular hyperpolarizability. It should be noted that the coefficients α_{ij}, β_{ijk}, and γ_{ijkl} are frequency dependent.

The tensor averages of the microscopic (hyper) polarizabilities form the macroscopic susceptibilities tensors. Depending on the alignment of the field, each element in the susceptibilities relates to an orientational averaging of the (hyper) polarizabilities. Regarding this, the isotropic second hyperpolarizability is defined as [20],

$$\langle\gamma(-\omega;\omega,-\omega,\omega)\rangle = \frac{1}{15}\sum_{\alpha=\{x,y,z\}}\sum_{\beta=\{x,y,z\}}\left(\gamma_{\alpha\alpha\beta\beta}+\gamma_{\alpha\beta\alpha\beta}+\gamma_{\alpha\beta\beta\alpha}\right) \tag{50}$$

For two degenerate linearly polarized photons, the TPA cross section can be calculated as

$$\sigma_{TPA}(\omega) = \frac{N\pi^3\alpha_f^2\omega^2\hbar^3}{15e^4}\sum_{\alpha=\{x,y,z\}}\sum_{\beta=\{x,y,z\}} Im\,[\gamma_{\alpha\alpha\beta\beta}(-\omega;\omega,\omega,-\omega) + \gamma_{\alpha\beta\beta\alpha}(-\omega;\omega,\omega,-\omega)+\gamma_{\alpha\beta\alpha\beta}(-\omega;\omega,\omega,-\omega)] \tag{51}$$

where α_f is the fine structure constant and N is an integer value related to the experimental setup [21,22]. The σ_{TPA} unit is Goeppert-Mayer ($1GM = 10^{-50} cm^4 s\ photon^{-1}$).

3. MATERIALS AND METHOD

3.1 Molecular Design

In order to get an efficient TPA cross section, the structural design of molecules is very crucial. It has been investigated that electron donors and acceptors as well as conjugated bridges are necessary for large TPA cross sections. Moreover, large hyperpolarizability is observed for systems with significant charge-transfer transitions, so the TPA and intramolecular charge-transfer are correlated. The presence of donors, acceptors, and coplanarity in organic molecules can enhance charge-transfer and, as a result, can improve TPA. When charge-transfer increases, it leads to a larger dipole moment and consequently, a better TPA cross section. Therefore, the main characteristics of organic molecules which can have a significant effect on TPA cross sections include long, π-conjugated molecules with donor (D) and acceptor (A) substituents and a small HOMO-LUMO gap to enhance hyperpolarizability.

In this thesis, we studied four molecules with a sulfur (S) atom which links donors, acceptors, or mixed species. Our hypothesis is based on the fact that the sulfur atom can act either as a donor or an acceptor to increase TPA, depending on the molecular system.

Our studied systems are acceptor/donor-substituted diphenyl thioethers (ASA, DSD, DSA) and N-protonated p-methoxyphenyl-4-pyridine ($DSAPh^+$) . ASA, DSD, DSA and $DSAPh^+$ are shown in Figure 6–9, respectively.

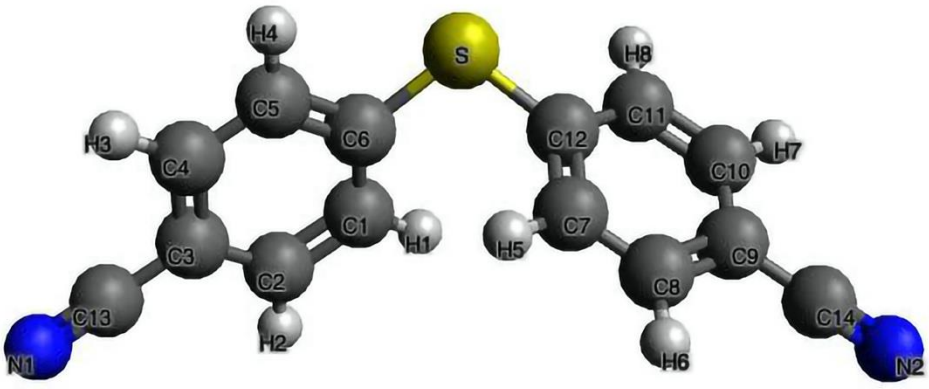

Figure 6. *Acceptor-Sulfur-Acceptor (ASA) molecular system*

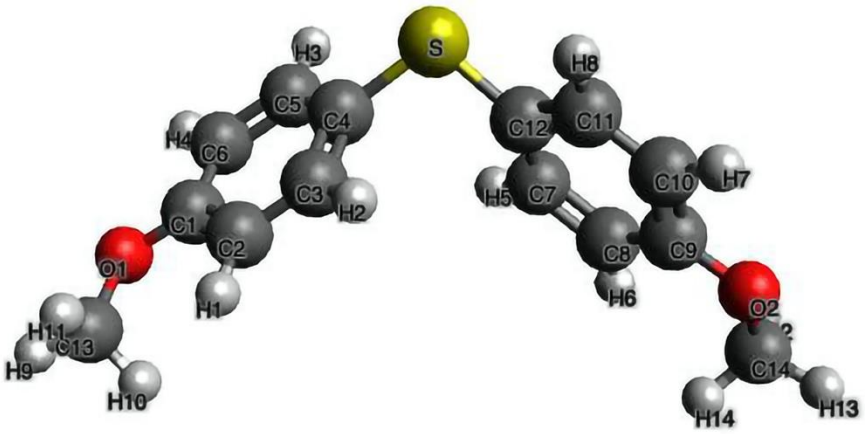

Figure 7. *Donor-Sulfur-Donor (DSD) molecular system*

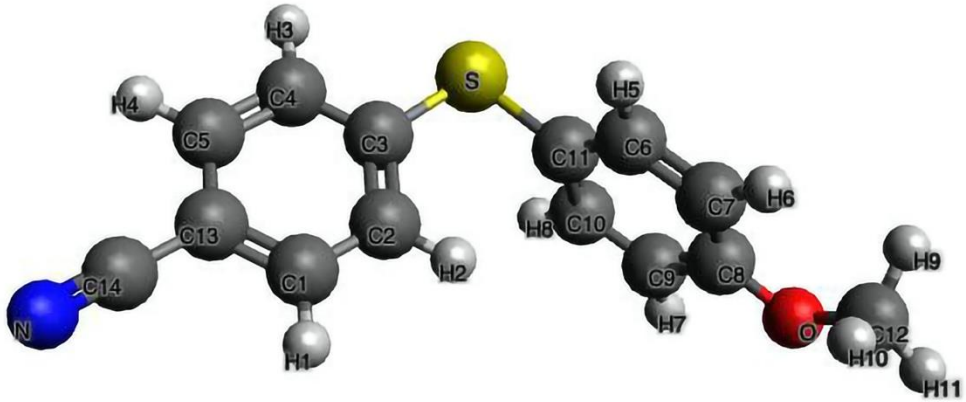

Figure 8. *Donor-Sulfur-Acceptor (DSA) molecular system*

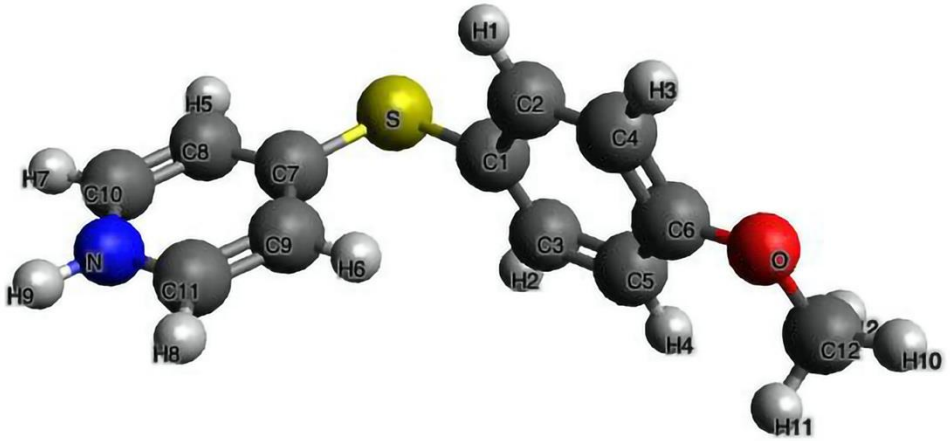

Figure 9. *N-Protonated Donor-Sulfur-Acceptor ($DSAPh^{+}$) molecular system*

3.2 Exchange-Correlation Functional and Basis Set

Choosing the most appropriate basis set and functional is not a trivial job. This choice can greatly affect the accuracy of the results. Regarding the basis set, it should be large enough to reveal the electronic structure of the studied molecules properly. There are a lot of classifications for basis sets. In this thesis, we chose def2-TZVP which belongs to the Ahlriches-Weigend basis set family. It is a valence triple zeta plus polarization basis set that is relatively large. This basis set is quite accurate and suitable for computational calculations [23].

Considering the functionals, the choice depends on the studied molecules and our desired accuracy. We have a large variety of functionals such as hybrid, range-separated, and so on. In this thesis, we chose CAM-B3LYP for the computation [24,25]. B3LYP is a Becke three-parameter hybrid functional which is improved by the long-range correction. CAM-B3LYP is one of the most commonly used functionals for calculating the TPA spectra.

4. RESULTS AND DISCUSSION

Prior to performing our computations, we carried out the geometry optimizations with the Gaussian'09 [26] software package. Geometry optimization is necessary to minimize the total energy of the system and it is essential for calculating physical and chemical properties of our molecular systems. We obtained the coordinates of the optimized geometry at CAM-B3LYP/def2-TZVP level of theory. The results can be found in Appendix A, Table A1–A4.

Next, we started out our TPA calculations using ADF (Amsterdam Density Functional) product of SCM-AMS (Amsterdam Modelling Suite) [27]. ADF is a very well-designed quantum chemistry software package, which uses Slater Type Orbitals (STOs). However, during our calculations, we had issues in the calculation of the TPA cross sections using hybrid exchange-correlation functionals. Although the incident was reported to SCM, it remained unresolved until the completion of the thesis.

Another software package we used to calculate TPAs was GAMESS-US [28]. However, GAMESS-US does not have def2-TZVP implemented at the time of the writing of this thesis. To overcome this problem, we manually imported the necessary basis set information obtained from https://www.basissetexchange.org [29]. We started out our TPA calculations at CAM-B3LYP/def2-TZVP level of theory. We encountered significant slowdowns during the calculations after calculating several excited states (after the first 10 states, generally). It almost slowed down to a halt. As a result, we were unable to finish the calculations in time. However, we managed to finish one TPA calculation with PBE0/def2-TZVP level of theory for ASA molecule.

We also tried DALTON [30] to calculate the TPA cross sections. The reported cross sections are carried out using DALTON. Unfortunately, PBE0 functional was not implemented at the time of the writing of this thesis, so we didn't have a chance to compare the results with GAMESS-US. We started our calculations using the optimized geometries obtained from Gaussian'09 software package at the CAM-BL3LYP/def2-TZVP level of theory. The TPA cross sections were also calculated at the same level of theory. Due to the lack of implementations of TPA in quantum chemistry software packages, we could not cross-check our results with other software packages. So, we decided to carry out a Coupled-Cluster (CC) calculation to be used as a reference calculation; however, at the time of the writing of this thesis, there existed only the serial implementation of the method. So, we were left to use Møller–Plesset perturbation theory of second order (MP2). However, the calculations required more than 300 GB of memory, for which we didn't have the computational resources.

To find the TPA cross sections (σ_{TPA}) for our molecules, we first figured out the one-photon excitation energies through the Time-Dependent Density Functional Theory (TDDFT) [31], using Gaussian'09 software package. We performed the calculations at the CAM-B3LYP/def2-TZVP level of theory for

50 singlet states. We then used the half of the one-photon excitation energies to calculate the TPA cross sections. Having calculated the OPA and TPA spectra for 50 singlet excited states, we plotted the resulting spectra in Figure 10–13 for ASA, DSD, DSA, and $DSAPh^{+}$, respectively.

Figure 10–13 employ two distinct scales to present the spectra. The left scale corresponds to the TPA cross section σ_{TPA} given in GM units, while the right scale represents the molar extinction coefficient for OPA given in per mole per cm. In all these figures, the green curves represent the TPA cross section when the incident light is circularly polarized, while the magenta curves represent the TPA cross section under linear polarization. The blue curves, on the other hand, represent the molar extinction coefficient for OPA. The inclusion of OPA allows the comparison of energies associated with the excitations. We should also mention that, in Figure 10 and Figure 13, we chopped the peaks located at energies around 4 eV for visual convenience.

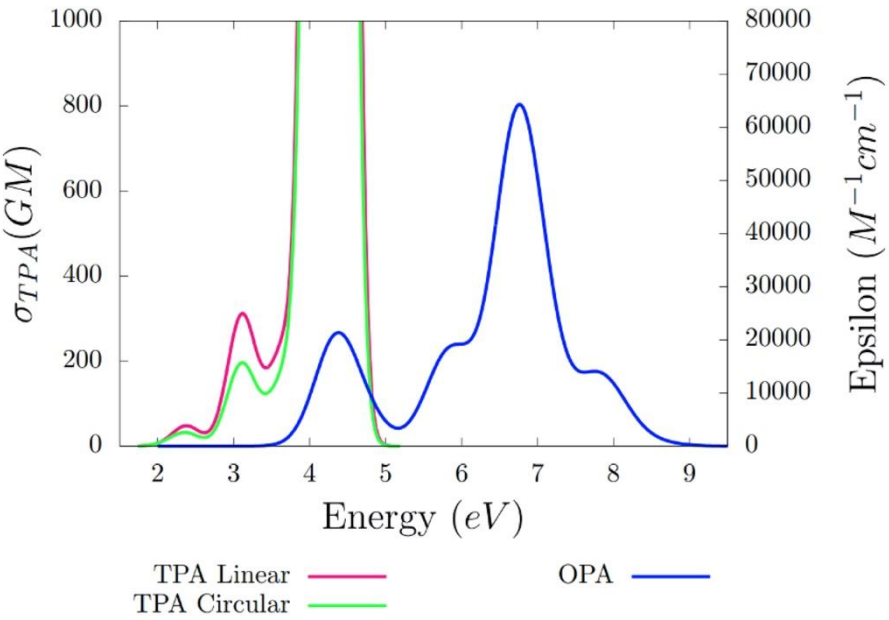

Figure 10. *ASA spectra*

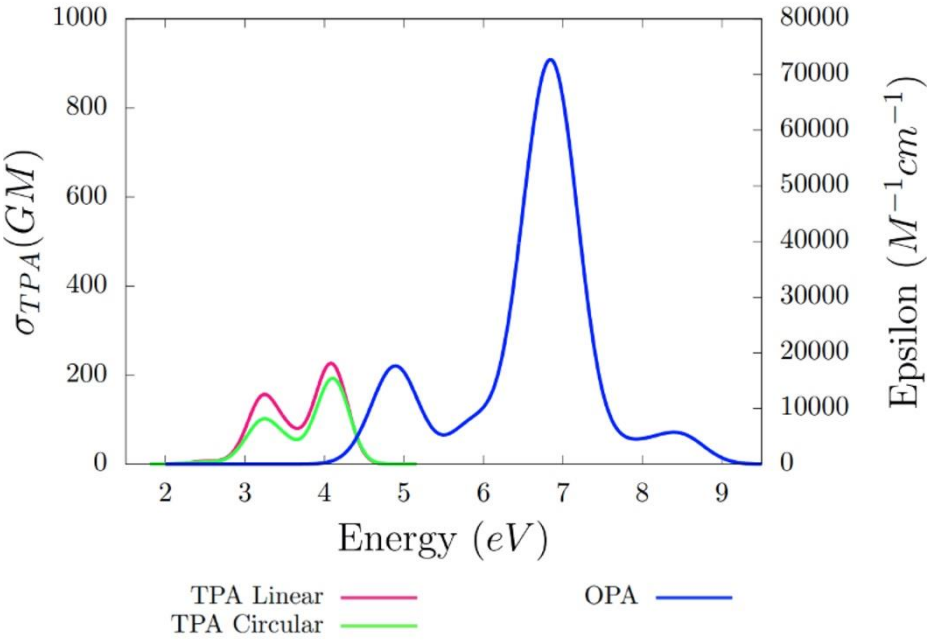

Figure 11. *DSD spectra*

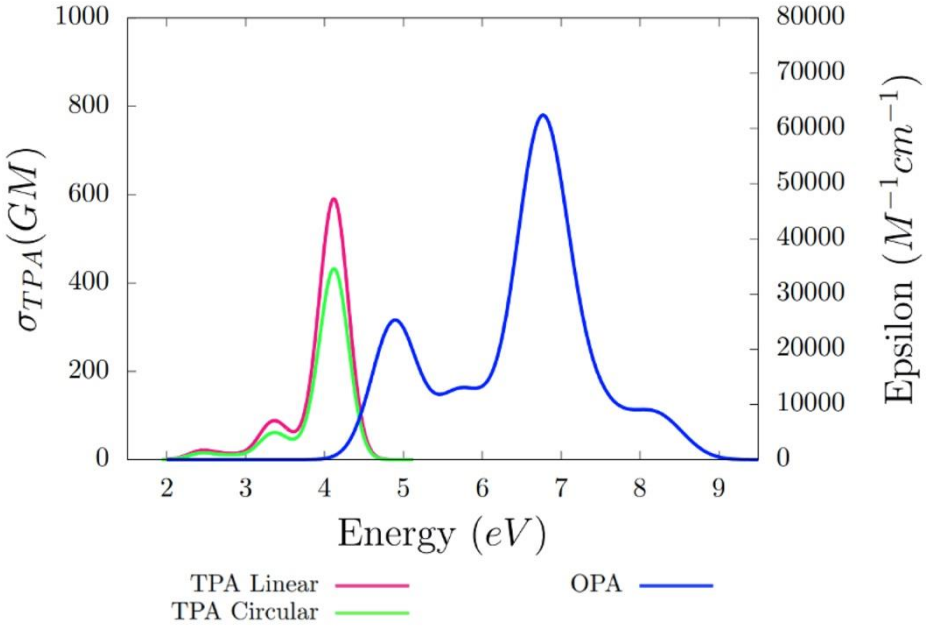

Figure 12. *DSA spectra*

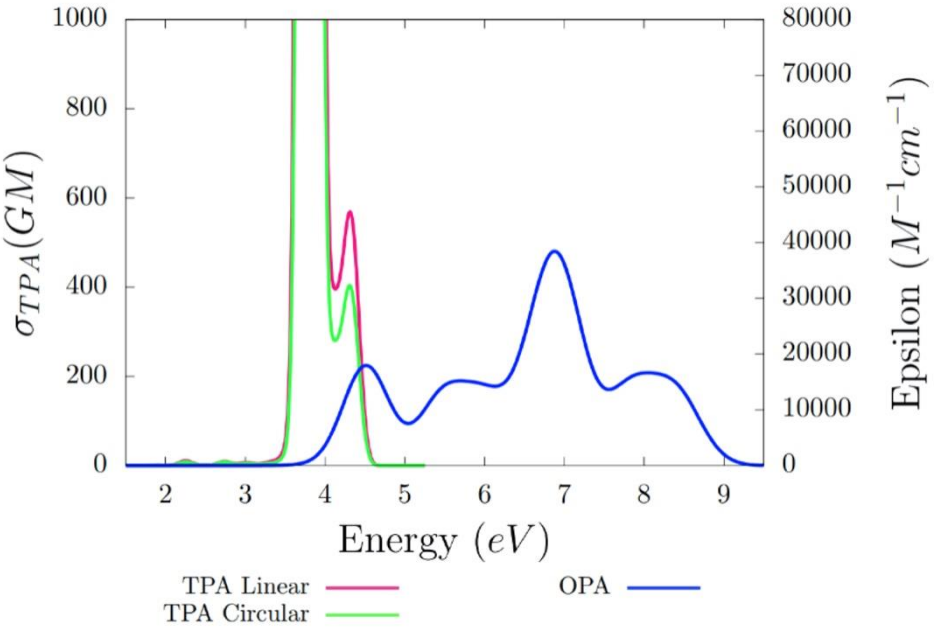

Figure 13. *$DSAPh^+$ spectra*

Regarding these results, ASA and $DSAPh^+$, as seen in Figure 10 and 13, show large TPA cross sections at specific energies. TPA for ASA becomes maximum at 4.28 eV with values $1.88 \times 10^4\ GM$ and $1.23 \times 10^4\ GM$ for linearly and circularly polarized light, respectively. Also, TPA for $DSAPh^+$ becomes maximum at 3.8 eV with values $1.67 \times 10^4 GM$ and $1.13 \times 10^4 GM$ for linearly and circularly polarized light, respectively. As for DSD and DSA, we do not observe such large TPA cross sections. The full list of TPA cross sections for these four molecules are tabulated in Appendix B: *TPA Cross Section Tables*, Table B1–B8. We should also mention that gaussian envelope is used to obtain the spectra given in Figure 10–13.

In the next step, we analyzed the results using Natural Transition Orbitals (NTOs) [32], which help us to have a more intuitive understanding of the orbitals and electronic transitions. The NTOs are obtained by applying distinct unitary transformations on both the occupied and virtual orbitals. This gives us a localized representation of the transition density matrix.

Here, we represent the NTOs of the strongest TPA transitions for our four molecules. Figure 14–17 and Table 1–4 show the NTOs and the strongest TPA transitions for ASA, DSD, DSA, and $DSAPh^+$, respectively. In Figure 14–17, the left side represents the orbitals corresponding to the holes, while the right side represents the orbitals for the particles.

Figure 14, representing the ASA molecule, displays a notable electron localization on the sulfur atom within the hole orbital. Conversely, in the particle orbital, there is a significant electron depletion on

the sulfur atom and delocalization on both phenyl groups. This indicates that the sulfur atom is an effective donor in this case.

ASA: 64% occupation

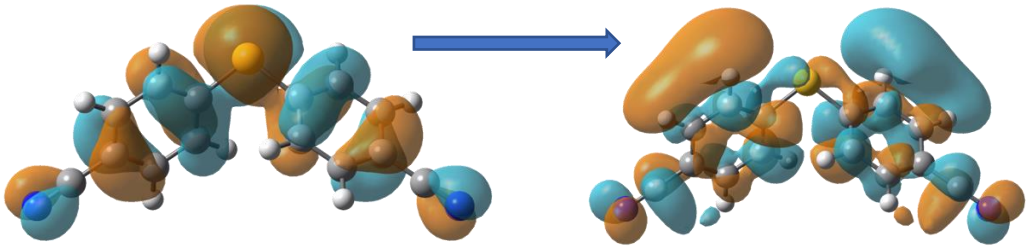

Figure 14. *The NTO of the strongest TPA transition for ASA*

TPA $E(eV)$	$\lambda(nm)$	f	$\sigma_{TPA}(GM)$ Linear/Circular
4.28	289.7	0.0001	18800/12700

Table 1. *The strongest TPA transition for ASA*

DSD: 62% occupation

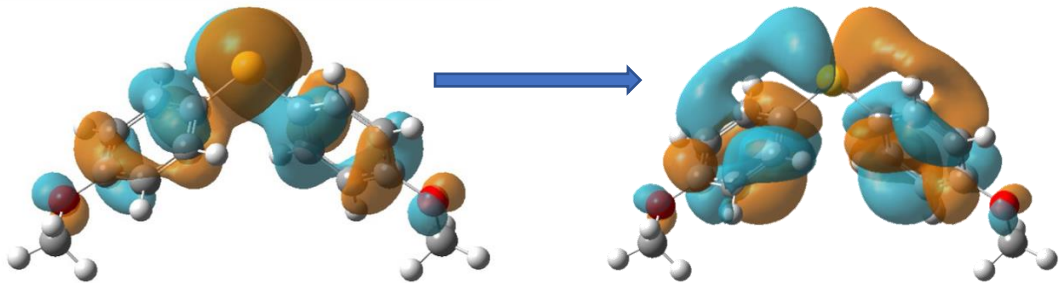

Figure 15. *The NTO of the strongest TPA transition for DSD*

TPA $E(eV)$	$\lambda(nm)$	f	$\sigma_{TPA}(GM)$ Linear/Circular
3.26	380.3	0.0164	123/70

Table 2. *The strongest TPA transition for DSD*

In Figure 15, which represents the *DSD* molecule, we see a significant charge localization on the sulfur atom in the hole orbital. When we look at the particle orbital, although there is a charge delocalization over the phenyl group extending to cover the sulfur atom, there isn't significant charge depletion on the sulfur atom, hence the TPA cross section is considerably low. We should also point out that in *DSD*

molecule, the oscillator strength f associated with the transition corresponding to the largest TPA cross section is significantly higher than that of the ASA molecule. This shows that excitation with a high oscillator strength does not necessarily render large TPA cross sections.

In Figure 16, representing the DSA molecule, we see a limited charge transfer. Initially, there is almost no charge localization on the phenyl ring with the methoxy group. However, after the excitation, we observe some shift of charge from the oxygen atom to carbon atom of the methoxy group and somehow increased presence of charge on the phenyl ring on the same side. The charge density on the phenyl ring on the nitrile group side essentially remains the same; however, a significant charge delocalization is observed on the sulfur atom extending to the space in between the phenyl rings. This behavior can be attributed to the large dihedral angle between planes defined by phenyl rings. Here, a low TPA cross section is observed again. We believe that this is due to the limited charge transfer facilitation, despite the fact that the oscillator strength is higher compared to any of the aforementioned molecules.

DSA: 48% occupation

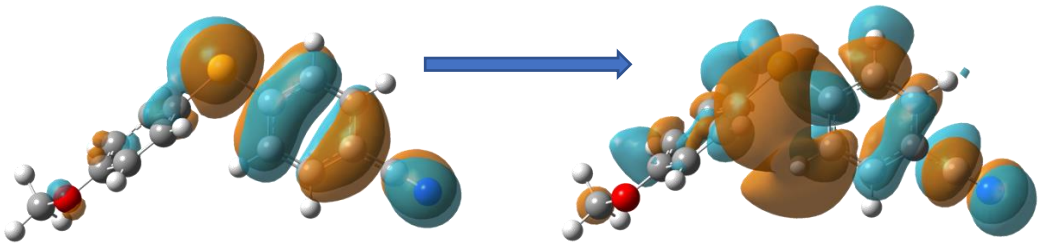

Figure 16. *The NTO of the strongest TPA transition for DSA*

TPA $E(eV)$	$\lambda(nm)$	f	$\sigma_{TPA}(GM)$ Linear/Circular
4.08	303.8	0.0281	217/140

Table 3. *The strongest TPA transition for DSA*

In Figure 17, representing the $DSAPh^{+}$ molecule, we see a significant charge delocalization over the phenyl ring, accompanied by a charge depletion on the sulfur atom and a charge accumulation on the far side of the pyridine for this transition. The largest TPA cross section is observed at 3.81 eV with σ_{TPA} =16700 GM. The oscillator strength corresponding to this transition is almost similar to that of the DSD molecule, where the TPA cross section is much lower.

$DSAPh^+$: 90% occupation

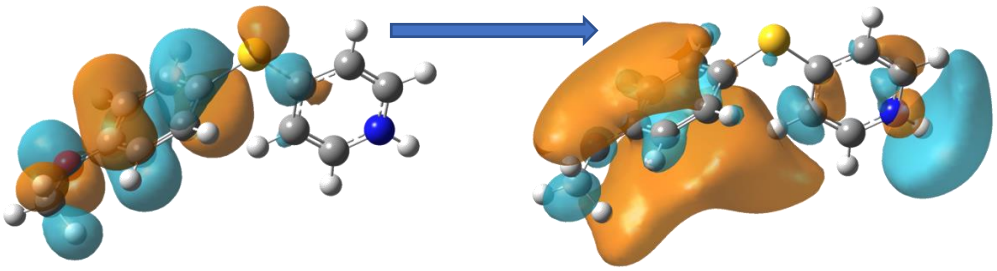

Figure 17. *The NTO of the strongest TPA transition for* $DSAPh^+$

TPA $E(eV)$	$\lambda(nm)$	f	$\sigma_{TPA}(GM)$ Linear/Circular
3.81	325.4	0.0119	16700/11300

Table 4. *The strongest TPA transition for* $DSAPh^+$

5. CONCLUSION

In this study, we have explored a new structural (design) principle in search of small molecules with large TPA cross sections. Sulfur is used as a bridge in these molecules by connecting donor, acceptor, or mixed π systems. For the geometry optimizations and TPA calculations, we used DFT at the CAM-B3LYP/def2-TZVP level of theory. We studied four small molecules in order to investigate if they could be good candidates for TPA processes such as photodynamic therapy to target tumors. Our systems have a relatively short conjugation length and we have only one conjugation path in them. In our calculations, we find that ASA and $DSAPh^{+}$ molecules have the largest TPA cross sections compared to those of DSA and DSD molecules. Considering the results for our molecules, we need ultra-violet lasers, for which, depending on the desired application, we need to work further on the design to lower the required input energy. Moreover, we can study solvent effects on our systems. Solvents can affect the electronic structure of the molecule and, therefore, have a significant influence on the TPA cross sections. The lack of implementations of TPA processes in quantum chemistry software packages has been a great obstacle during this project. However, we believe that, in time, these issues will be resolved.

REFERENCES:

[1] M. Göppert-Mayer, "Über Elementarakte mit zwei Quantensprüngen," *Ann. Phys.*, vol. 401, no. 3, pp. 273–294, 1931.

[2] W. Kaiser and C. G. B. Garrett, "Two-Photon Excitation in CaF2:Eu2+," *Phys. Rev. Lett.*, vol. 7, no. 6, pp. 229–231, 1961.

[3] C. N. LaFratta, J. T. Fourkas, T. Baldacchini, and R. A. Farrer, "Multiphoton fabrication," *Angew. Chem. Int. Ed Engl.*, vol. 46, no. 33, pp. 6238–6258, 2007.

[4] V. Harinarayana and Y. C. Shin, "Two-photon lithography for three-dimensional fabrication in micro/nanoscale regime: A comprehensive review," *Opt. Laser Technol.*, vol. 142, no. 107180, p. 107180, 2021.

[5] A. S. Dvornikov, E. P. Walker, and P. M. Rentzepis, "Two-photon three-dimensional optical storage memory," *J. Phys. Chem. A*, vol. 113, no. 49, pp. 13633–13644, 2009.

[6] F. Helmchen and W. Denk, "Erratum: Corrigendum: Deep tissue two-photon microscopy," *Nat. Methods*, vol. 3, no. 3, pp. 235–235, 2006.

[7] W. R. Zipfel, R. M. Williams, and W. W. Webb, "Nonlinear magic: multiphoton microscopy in the biosciences," *Nat. Biotechnol.*, vol. 21, no. 11, pp. 1369–1377, 2003.

[8] J. D. Bhawalkar, N. D. Kumar, C. F. Zhao, and P. N. Prasad, "Two-photon photodynamic therapy," *J. Clin. Laser Med. Surg.*, vol. 15, no. 5, pp. 201–204, 1997.

[9] Z. Sun, L.-P. Zhang, F. Wu, and Y. Zhao, "Photosensitizers for two-photon excited photodynamic therapy," *Adv. Funct. Mater.*, vol. 27, no. 48, p. 1704079, 2017.

[10] I. Probodh and D. Thomas, *Two-photon excitation photodynamic therapy: Working toward a new treatment for wet age-related macular degeneration," in Age Related Macular Degeneration - The Recent Advances in Basic Research and Clinical Care*. InTech, 2012.

[11] F. Terenziani, C. Katan, E. Badaeva, S. Tretiak, and M. Blanchard-Desce, "Enhanced two-photon absorption of organic chromophores: Theoretical and experimental assessments," *Adv. Mater.*, vol. 20, no. 24, pp. 4641–4678, 2008.

[12] G. S. He, L.-S. Tan, Q. Zheng, and P. N. Prasad, "ChemInform abstract: Multiphoton absorbing materials: Molecular designs, characterizations, and applications," *ChemInform*, vol. 39, no. 24, 2008.

[13] M. Pawlicki, H. A. Collins, R. G. Denning, and H. L. Anderson, "Two-photon absorption and the design of two-photon dyes," *Angew. Chem. Int. Ed Engl.*, vol. 48, no. 18, pp. 3244–3266, 2009.

[14] A. Szabo and N. S. Ostlund, Modern quantum chemistry: Introduction to advanced electronic structure theory. Dover Publications, 2012.

[15] P. W. Atkins and R. S. Friedman, Molecular Quantum Mechanics, 4th ed. London, England: Oxford University Press, 2004.

[16] F. Jensen, Introduction to computational chemistry, 2nd ed. Hoboken, NJ: Wiley-Blackwell, 2006.

[17] P. Hohenberg and W. Kohn, "Inhomogeneous Electron Gas," Phys. Rev., vol. 136, no. 3B, pp. B864–B871, 1964.

[18] W. Kohn and L. J. Sham, "Self-consistent equations including exchange and correlation effects," Phys. Rev., vol. 140, no. 4A, pp. A1133–A1138, 1965.

[19] "Density functional (DFT) methods." [Online]. Available: https://gaussian.com/dft/.

[20] K. Ahmadzadeh et al., "Efficient implementation of isotropic cubic response functions for two-photon absorption cross sections within the self-consistent field approximation," J. Chem. Phys., vol. 154, no. 2, p. 024111, 2021.

[21] Z. Hu, J. Autschbach, and L. Jensen, "Simulating third-order nonlinear optical properties using damped cubic response theory within time-dependent density functional theory," J. Chem. Theory Comput., vol. 12, no. 3, pp. 1294–1304, 2016.

[22] Z. Hu and L. Jensen, "A discrete interaction model/quantum mechanical method for simulating plasmon-enhanced two-photon absorption," J. Chem. Theory Comput., vol. 14, no. 11, pp. 5896–5903, 2018.

[23] F. Weigend and R. Ahlrichs, "Balanced basis sets of split valence, triple zeta valence and quadruple zeta valence quality for H to Rn: Design and assessment of accuracy," Phys. Chem. Chem. Phys., vol. 7, no. 18, pp. 3297–3305, 2005.

[24] M. Chołuj et al., "Choosing bad versus worse: Predictions of two-photon-absorption strengths based on popular density functional approximations," J. Chem. Theory Comput., vol. 18, no. 2, pp. 1046–1060, 2022.

[25] T. Yanai, D. P. Tew, and N. C. Handy, "A new hybrid exchange–correlation functional using the Coulomb-attenuating method (CAM-B3LYP)," Chem. Phys. Lett., vol. 393, no. 1–3, pp. 51–57, 2004.

[26] M. J. Frisch, G. W. Trucks, H. B. Schlegel, G. E. Scuseria, M. A. Robb, J. R. Cheeseman, G. Scalmani, V. Barone, G. A. Petersson, H. Nakatsuji, X. Li, M. Caricato, A. Marenich, J. Bloino, B. G. Janesko, R. Gomperts, B. Mennucci, H. P. Hratchian, J. V. Ortiz, A. F. Izmaylov, J. L. Sonnenberg, D. Williams-Young, F. Ding, F. Lipparini, F. Egidi, J. Goings, B. Peng, A. Petrone, T. Henderson, D. Ranasinghe, V. G. Zakrzewski, J. Gao, N. Rega, G. Zheng, W. Liang, M. Hada, M. Ehara, K. Toyota, R. Fukuda, J. Hasegawa, M. Ishida, T. Nakajima, Y. Honda, O. Kitao, H.

Nakai, T. Vreven, K. Yrossell, J. A. Montgomery, J. E. Peralta, F. Ogliaro, M. Bearpark, J. J. Heyd, E. Brothers, K. N. Kudin, V. N. Staroverov, T. Keith, R. Kobayashi, J. Normand, K. Raghavachari, A. Rendell, J. C. Burant, S. S. Iyengar, J. Tomasi, M. Cossi, J. M. Millam, M. Klene, C. Adamo, R. Cammi, J. W. Ochterski, R. L. Martin, K. Morokuma, O. Farkas, J. B. Foresman, and D. J. Fox, Gaussian, Inc. , Wallingford CT, " Gaussian 09." 2016.

[27] G. Velde et al., "Chemistry with ADF," vol. 22, 2001.

[28] M. W. Schmidt et al., "General atomic and molecular electronic structure system," J. Comput. Chem., vol. 14, no. 11, pp. 1347–1363, 1993.

[29] "Basis Set Exchange (BSE)," Basissetexchange.org. [Online]. Available: https://www.basissetexchange.org/.

[30] K. Aidas et al., "The Dalton quantum chemistry program system: The Dalton program," Wiley Interdiscip. Rev. Comput. Mol. Sci., vol. 4, no. 3, pp. 269–284, 2014.

[31] T. Tsuneda, Density functional theory in quantum chemistry, 2014th ed. Tokyo, Japan: Springer, 2014.

[32] R. L. Martin, "Natural transition orbitals," J. Chem. Phys., vol. 118, no. 11, pp. 4775–4777, 2003.

APPENDICES :

A. Optimized Geometry Tables

Element	x	y	z
C	-1.45001300	-0.19991800	-0.81347700
C	-2.59039900	-0.97385900	-0.83928900
C	-3.70065300	-0.60783200	-0.08196500
C	-3.65226700	0.53625200	0.70582900
C	-2.50088500	1.29788300	0.74527000
C	-1.39460700	0.93727800	-0.01430400
H	-0.59977500	-0.47861300	-1.41978400
H	-2.63282800	-1.85970100	-1.45752000
H	-4.51257800	0.81841900	1.29636300
H	-2.45576000	2.17564600	1.37535400
C	1.45006500	-0.19985300	0.81357100
C	2.59045600	-0.97378400	0.83936600
C	3.70065800	-0.60780800	0.08193800
C	3.65221200	0.53619800	-0.70595600
C	2.50081400	1.29781900	-0.74538400
C	1.39460600	0.93728000	0.01430800
H	0.59986400	-0.47851700	1.41994300
H	2.63292900	-1.85957800	1.45766500
H	4.51247700	0.81832400	-1.29657600
H	2.45562400	2.17550800	-1.37556500
S	-0.00000700	2.02485300	0.00003600
C	-4.88660100	-1.40801700	-0.11487700
C	4.88664000	-1.40794900	0.11484100
N	-5.83586500	-2.04938400	-0.14099800
N	5.83586400	-2.04937000	0.14104400

Table A1. *Coordinates of the optimized geometry of ASA at CAM-B3LYP/def2-TZVP level of theory*

Element	x	y	z
C	-3.65578000	-0.48484300	-0.13351500
C	-2.68839900	-0.68321900	0.84397500
C	-1.57163100	0.13567100	0.88218400
C	-1.38766900	1.13729400	-0.05680000
C	-2.35821400	1.32108900	-1.03669000
C	-3.48515400	0.52729700	-1.07083700
H	-2.79745900	-1.45965000	1.58599700
H	-0.83113100	-0.01499900	1.65628100
H	-2.22228900	2.09449800	-1.78086500
H	-4.24456600	0.66667500	-1.82802100
C	1.57163200	0.13567300	-0.88218500
C	2.68840100	-0.68321600	-0.84397700
C	3.65578000	-0.48484300	0.13351600
C	3.48515200	0.52729500	1.07083900
C	2.35821200	1.32108700	1.03669200
C	1.38766900	1.13729400	0.05680000
H	0.83113400	-0.01499500	-1.65628500
H	2.79746100	-1.45964600	-1.58600100
H	4.24456300	0.66667100	1.82802500
H	2.22228600	2.09449500	1.78086900
S	0.00000000	2.24178500	0.00000000
O	-4.78613200	-1.22302200	-0.25130400
O	4.78613200	-1.22302200	0.25130500
C	-5.01413800	-2.25920900	0.67715600
H	-5.96334000	-2.70995300	0.40051600
H	-4.22833700	-3.01767100	0.63064800
H	-5.08268100	-1.87349700	1.69755800
C	5.01413900	-2.25920700	-0.67715700
H	5.08268400	-1.87349300	-1.69755900
H	5.96334100	-2.70995200	-0.40051700
H	4.22833800	-3.01766900	-0.63065300

Table A2. *Coordinates of the optimized geometry of DSD at CAM-B3LYP/def2-TZVP level of theory*

Element	x	y	z
C	2.52953800	-1.26644300	0.07514200
C	1.41760400	-0.44833800	0.04202300
C	1.56588600	0.92815900	-0.07302600
C	2.84743800	1.47186600	-0.15430700
C	3.95644600	0.65711100	-0.12240200
H	2.40938400	-2.33726200	0.16529500
H	0.43208600	-0.88526000	0.10627700
H	2.97166300	2.54338700	-0.24294300
H	4.94731900	1.08492200	-0.18610700
C	-1.88168900	0.61036300	-1.10181800
C	-3.04167600	-0.14127100	-0.99463400
C	-3.54974800	-0.44185800	0.26276400
C	-2.89066700	0.01661300	1.40205900
C	-1.74146200	0.76343200	1.28231200
C	-1.21820800	1.06335700	0.02589600
H	-1.48854400	0.84733100	-2.08123400
H	-3.53684700	-0.47955800	-1.89188000
H	-3.30609700	-0.22228400	2.37130100
H	-1.23699100	1.12340900	2.16876900
S	0.22520300	2.07338000	-0.12934900
O	-4.66965400	-1.16274400	0.47891300
C	-5.38995900	-1.65041700	-0.63386100
H	-5.74867200	-0.83315900	-1.26394900
H	-4.78160300	-2.33158700	-1.23354300
H	-6.24029700	-2.19110600	-0.22841800
C	3.80655300	-0.72335900	-0.00692200
C	4.95558000	-1.57336500	0.02681000
N	5.87696200	-2.25515200	0.05350000

Table A3. *Coordinates of the optimized geometry of DSA at CAM-B3LYP/def2-TZVP level of theory*

Element	x	y	z
S	1.05478900	-1.68784100	-0.12510400
C	-0.52413800	-0.91563300	0.02689100
C	-1.08153800	-0.70308000	1.28815300
C	-1.25365000	-0.60247800	-1.10964600
C	-2.33792200	-0.16097300	1.40179800
H	-0.52968600	-0.97378700	2.17844900
C	-2.52171400	-0.05977800	-1.00272100
H	-0.83660800	-0.79028700	-2.09010100
C	-3.07149000	0.16518700	0.25727800
H	-2.78992100	0.00765600	2.36916600
H	-3.07484900	0.17156300	-1.89974400
C	2.18783100	-0.39478900	-0.06641000
C	3.55404000	-0.72659200	-0.15500100
C	1.84837700	0.96123300	0.06394900
C	4.49510400	0.25291900	-0.11272600
H	3.86562800	-1.75651800	-0.25599100
C	2.83198400	1.90242800	0.10128700
H	0.81568400	1.26613300	0.13561500
H	5.55499900	0.05536300	-0.17599500
H	2.62918200	2.95878300	0.20048100
H	4.83836100	2.25794700	0.04464700
O	-4.28623200	0.67814900	0.47126500
C	-5.11338800	1.00105100	-0.63651600
H	-6.03804000	1.38176000	-0.21502700
H	-4.65327000	1.77122800	-1.25824600
H	-5.32538800	0.11522000	-1.23756000
N	4.12516600	1.54260400	0.01397500

Table A4. *Coordinates of the optimized geometry of $DSAPh^+$ at CAM-B3LYP/def2-TZVP level of theory*

B. TPA Cross Section Tables

$E(eV)$	$\sigma_{TPA}(GM)$
2.18	4.80
2.37	3.96×10^{1}
2.40	5.10×10^{-2}
2.53	8.45
2.88	6.99×10^{-2}
2.91	3.01
3.00	9.27×10^{1}
3.01	7.71
3.15	2.25×10^{2}
3.33	2.28×10^{-2}
3.35	2.31
3.35	1.48×10^{-1}
3.40	4.83
3.40	1.68
3.42	7.48×10^{-2}
3.43	1.06×10^{1}
3.47	9.92×10^{-1}
3.53	6.32×10^{1}
3.54	1.51
3.55	1.51
3.61	1.54
3.61	2.12×10^{-1}
3.69	1.48×10^{2}
3.80	3.41
3.83	6.10×10^{-2}
3.83	1.84
3.84	2.30
3.87	2.64
3.87	1.06×10^{1}
3.89	6.94
3.91	5.63
3.92	3.06
3.93	2.63
3.97	1.22
3.98	1.74
3.98	4.48×10^{-1}
4.00	1.42×10^{1}
4.04	1.38×10^{2}
4.06	1.10×10^{2}
4.06	5.00×10^{1}
4.10	8.08×10^{1}
4.11	1.92×10^{1}
4.13	3.09×10^{1}
4.13	7.34
4.18	5.39
4.20	9.97×10^{1}
4.21	1.33×10^{2}
4.25	1.96×10^{2}
4.28	1.88×10^{4}
4.33	1.61×10^{2}

Table B1. *One-photon excitation energies and corresponding TPA cross sections (linear) for ASA at CAM-B3LYP/def2-TZVP level of theory*

$E(eV)$	$\sigma_{TPA}(GM)$
2.18	7.19
2.37	2.48×10^{1}
2.40	7.65×10^{-2}
2.53	4.91
2.88	1.05×10^{-1}
2.91	2.00
3.00	5.97×10^{1}
3.01	1.16×10^{1}
3.15	1.32×10^{2}
3.33	3.41×10^{-2}
3.35	1.29
3.35	2.22×10^{-1}
3.40	7.25
3.40	2.24
3.42	6.93×10^{-2}
3.43	1.59×10^{1}
3.47	2.58×10^{-1}
3.53	2.61×10^{1}
3.54	2.27
3.55	2.26
3.61	7.63×10^{-1}
3.61	3.17×10^{-1}
3.69	1.06×10^{2}
3.80	5.11
3.83	9.15×10^{-2}
3.83	2.76
3.84	1.77
3.87	3.96
3.87	8.56
3.89	1.04×10^{1}
3.91	2.67
3.92	1.41
3.93	3.94
3.97	1.04
3.98	1.36
3.98	6.72×10^{-1}
4.00	6.76
4.04	2.06×10^{2}
4.06	1.65×10^{2}
4.06	3.36×10^{1}
4.10	1.21×10^{2}
4.11	1.32×10^{1}
4.13	1.32×10^{1}
4.13	1.10×10^{1}
4.18	8.08
4.20	4.23×10^{1}
4.21	1.99×10^{2}
4.25	2.93×10^{2}
4.28	1.27×10^{4}
4.33	2.41×10^{2}

Table B2. *One-photon excitation energies and corresponding TPA cross sections (circular) for ASA at CAM-B3LYP/def2-TZVP level of theory*

$E(eV)$	$\sigma_{TPA}(GM)$
2.255	2.96×10^{-1}
2.35	3.74×10^{-1}
2.425	3.65×10^{-1}
2.525	5.55
2.93	1.88
2.935	1.97
3.02	1.68×10^{1}
3.075	5.73
3.225	1.23×10^{2}
3.275	1.40
3.305	1.58
3.39	2.53
3.41	3.59
3.45	1.54×10^{-1}
3.46	7.35
3.48	7.79
3.505	1.92×10^{1}
3.55	3.73
3.57	1.83×10^{1}
3.6	1.50
3.635	2.41
3.64	5.81×10^{-2}
3.695	2.32×10^{-1}
3.72	1.09
3.725	9.26×10^{-1}
3.79	1.91
3.83	1.25
3.885	8.37
3.895	1.15×10^{1}
3.905	3.23×10^{-1}
3.91	4.78
3.92	9.68×10^{-1}
3.95	2.50×10^{1}
3.965	1.12×10^{1}
3.995	3.32
4.02	1.11
4.035	1.97×10^{1}
4.045	3.14×10^{1}
4.05	6.61
4.06	1.20
4.115	5.59×10^{1}
4.14	9.32
4.16	3.10×10^{1}
4.17	3.41
4.22	1.05×10^{1}
4.22	2.86
4.245	1.73×10^{1}
4.25	9.81
4.265	6.83×10^{-1}
4.3	1.99

Table B3. *One-photon excitation energies and corresponding TPA cross sections (linear) for DSD at CAM-B3LYP/def2-TZVP level of theory*

$E(eV)$	$\sigma_{TPA}(GM)$
2.255	4.44×10^{-1}
2.35	4.31×10^{-1}
2.425	5.47×10^{-1}
2.525	3.73
2.93	2.83
2.935	2.81
3.02	1.25×10^{1}
3.075	8.60
3.225	7.01×10^{1}
3.275	2.10
3.305	2.38
3.39	3.58
3.41	2.51
3.45	2.31×10^{-1}
3.46	1.10×10^{1}
3.48	4.03
3.505	1.06×10^{1}
3.55	5.59
3.57	6.17
3.6	2.25
3.635	1.04
3.64	8.71×10^{-2}
3.695	3.48×10^{-1}
3.72	1.64
3.725	5.40×10^{-1}
3.79	4.57×10^{-1}
3.83	1.87
3.885	5.48
3.895	7.50
3.905	4.84×10^{-1}
3.91	3.47
3.92	1.45
3.95	1.57×10^{1}
3.965	4.81
3.995	4.98
4.02	1.66
4.035	2.96×10^{1}
4.045	1.88×10^{1}
4.05	4.36
4.06	1.81
4.115	3.42×10^{1}
4.14	1.40×10^{1}
4.16	1.94×10^{1}
4.17	15.11
4.22	1.57×10^{1}
4.22	3.59
4.245	2.06×10^{1}
4.25	1.47×10^{1}
4.265	1.02
4.3	2.60

Table B4. *One-photon excitation energies and corresponding TPA cross sections (circular) for DSD at CAM-B3LYP/def2-TZVP level of theory*

$E(eV)$	$\sigma_{TPA}(GM)$
2.42	6.22
2.455	1.31×10^{1}
2.515	9.88×10^{-1}
2.585	2.41×10^{-2}
2.805	8.20
2.86	2.79
2.98	1.55×10^{-1}
3.08	9.79×10^{-1}
3.13	1.71×10^{-1}
3.255	5.88×10^{-1}
3.295	4.90×10^{1}
3.365	1.79×10^{1}
3.41	2.39
3.425	6.80×10^{-2}
3.49	2.64×10^{1}
3.525	3.14×10^{-1}
3.53	7.66×10^{-2}
3.555	5.68×10^{-1}
3.565	1.21×10^{-1}
3.67	2.91×10^{-2}
3.7	4.27
3.71	2.98
3.81	7.23×10^{-1}
3.835	1.74
3.845	5.06
3.855	3.33
3.88	2.02×10^{-1}
3.885	6.14×10^{-1}
3.905	1.54
3.92	1.33×10^{1}
3.935	9.00
3.955	2.28
3.965	6.70
3.97	4.30
3.98	8.19
4.01	7.29
4.025	1.51
4.06	3.89×10^{1}
4.08	2.17×10^{2}
4.1	4.46
4.13	6.90×10^{1}
4.145	5.20×10^{-1}
4.15	8.47×10^{-1}
4.16	1.04×10^{1}
4.165	4.67×10^{1}
4.17	1.07×10^{1}
4.18	1.45×10^{2}
4.23	1.55×10^{1}
4.26	1.30×10^{1}
4.27	1.01×10^{1}

Table B5. *One-photon excitation energies and corresponding TPA cross sections (linear) for DSA at CAM-B3LYP/def2-TZVP level of theory*

$E(eV)$	$\sigma_{TPA}(GM)$
2.42	4.36
2.455	9.44
2.515	6.78×10^{-1}
2.585	3.54×10^{-2}
2.805	5.21
2.86	3.14
2.98	1.28×10^{-1}
3.08	1.07
3.13	2.07×10^{-1}
3.255	3.97×10^{-1}
3.295	3.12×10^{1}
3.365	1.67×10^{1}
3.41	1.78
3.425	4.20×10^{-2}
3.49	1.46×10^{1}
3.525	4.51×10^{-1}
3.53	1.10×10^{-1}
3.555	7.16×10^{-1}
3.565	1.56×10^{-1}
3.67	4.03×10^{-2}
3.7	5.61
3.71	2.95
3.81	9.56×10^{-1}
3.835	1.33
3.845	3.49
3.855	2.36
3.88	2.16×10^{-1}
3.885	6.10×10^{-1}
3.905	1.91
3.92	9.27
3.935	7.73
3.955	1.78
3.965	5.26
3.97	3.14
3.98	5.40
4.01	4.95
4.025	2.09
4.06	3.04×10^{1}
4.08	1.40×10^{2}
4.1	5.90
4.13	5.89×10^{1}
4.145	3.52×10^{-1}
4.15	6.19×10^{-1}
4.16	6.16
4.165	3.22×10^{1}
4.17	6.78
4.18	1.15×10^{2}
4.23	1.14×10^{1}
4.26	9.22
4.27	7.98

Table B6. *One-photon excitation energies and corresponding TPA cross sections (circular) for DSA at CAM-B3LYP/def2-TZVP level of theory*

$E(eV)$	$\sigma_{TPA}(GM)$
1.9	4.82×10^{-1}
2.25	1.05×10^{1}
2.43	1.47×10^{-1}
2.46	5.90×10^{-1}
2.5	1.14×10^{-1}
2.635	1.81×10^{-1}
2.74	8.99
2.995	3.29×10^{-1}
3.005	5.06
3.02	9.38×10^{-1}
3.15	1.24
3.3	3.39
3.33	3.79
3.45	2.71
3.47	1.06
3.535	3.03×10^{-1}
3.54	2.45×10^{1}
3.55	1.99
3.56	1.09
3.595	7.66×10^{-1}
3.675	3.10×10^{-1}
3.76	1.01
3.79	6.52
3.805	1.67×10^{4}
3.815	1.70×10^{1}
3.825	4.95
3.86	3.15
3.875	4.71×10^{-1}
3.955	2.84×10^{1}
3.97	3.16
3.995	7.56×10^{-1}
4.045	6.90×10^{-1}
4.075	3.36×10^{1}
4.08	1.64×10^{2}
4.1	4.57×10^{1}
4.12	4.36×10^{1}
4.14	2.80
4.15	1.11×10^{1}
4.18	8.14
4.195	7.14
4.215	4.22×10^{1}
4.22	1.12×10^{1}
4.27	8.56×10^{1}
4.275	1.48×10^{2}
4.295	5.38×10^{1}
4.3	2.88
4.31	8.87×10^{-1}
4.37	1.08×10^{2}
4.37	1.97×10^{2}
4.375	1.93×10^{1}

Table B7. *One-photon excitation energies and corresponding TPA cross sections (linear) for $DSAPh^{+}$ at CAM-B3LYP/def2-TZVP level of theory*

$E(eV)$	$\sigma_{TPA}(GM)$
1.9	3.23×10^{-1}
2.25	8.00
2.43	1.22×10^{-1}
2.46	4.80×10^{-1}
2.5	1.09×10^{-1}
2.635	1.75×10^{-1}
2.74	8.10
2.995	2.06×10^{-1}
3.005	3.64
3.02	6.74×10^{-1}
3.15	1.31
3.3	2.11
3.33	2.40
3.45	1.07
3.47	8.91×10^{-1}
3.535	4.28×10^{-1}
3.54	1.52×10^{1}
3.55	2.12
3.56	8.97×10^{-1}
3.595	4.97×10^{-1}
3.675	4.30×10^{-1}
3.76	1.26
3.79	4.71
3.805	1.13×10^{4}
3.815	2.32×10^{1}
3.825	6.18
3.86	2.41
3.875	3.06×10^{-1}
3.955	1.88×10^{1}
3.97	2.52
3.995	6.10×10^{-1}
4.045	8.50×10^{-1}
4.075	3.74×10^{1}
4.08	1.01×10^{2}
4.1	2.84×10^{1}
4.12	2.92×10^{1}
4.14	3.39
4.15	1.26×10^{1}
4.18	9.40
4.195	9.16
4.215	2.32×10^{1}
4.22	5.79
4.27	5.45×10^{1}
4.275	9.30×10^{1}
4.295	7.13×10^{1}
4.3	4.10
4.31	8.96×10^{-1}
4.37	7.62×10^{1}
4.37	1.04×10^{2}
4.375	2.89×10^{1}

Table B8. *One-photon excitation energies and corresponding TPA cross sections (circular) for $DSAPh^{+}$ at CAM-B3LYP/def2-TZVP level of theory*

ÖZGEÇMİŞ

Name**: Shiva Mahmoudi**

MSc Physics	Marmara University, Istanbul, Turkey
BSc Physics	Azad University: Tehran Science and Research, Iran

CONFERENCES

- Poster presenter: “One-Photon and Two-Photon Absorption in Small organic Molecules”, Shiva Mahmoudi, Erdi Ata Bleda, Zikri Altun, Carl Trindle “The 38th International Physics Conference” organized by Turkish Physical Society, Bodrum, Turkey, 2022